

Effect of a calcium cathode on water-based nanoparticulate solar cells

Ben Vaughan, Andrew Stapleton, Bofei Xue, Elisa Sesa, Xiaojing Zhou, Glenn Bryant, Warwick Belcher, and Paul Dastoor^{a)}

Centre for Organic Electronics, University of Newcastle, Callaghan, NSW 2308, Australia

(Received 19 April 2012; accepted 29 June 2012; published online 30 July 2012)

Water-based nanoparticulate (NP) and bulk heterojunction (BHJ) organic photovoltaic (OPV) devices based on blends of poly(9,9-dioctylfluorene-co-N,N-bis(4-butylphenyl)-N,N-diphenyl-1,4-phenylenediamine) (PFB) and poly(9,9-dioctylfluorene-co-benzothiadiazole) (F8BT) have been fabricated with aluminium and calcium/aluminium cathodes. The NP devices exhibit power conversion efficiencies (PCEs) that are double that of the corresponding BHJ device. Moreover, the addition of calcium into the cathode structure results in a dramatic increase in open circuit voltage and PCEs approaching 1% for water-based polyfluorene OPV devices. © 2012 American Institute of Physics. [<http://dx.doi.org/10.1063/1.4737640>]

It is widely recognized that conventional organic photovoltaic (OPV) materials offer the prospect of low-cost fabrication using reel-to-reel manufacturing techniques.¹ However, two key aspects of current OPV fabrication are not well-suited to building large area PV modules using high speed printing. First, using current fabrication approaches to control phase segregation across large areas is problematic.² Second, using toxic, volatile, and flammable organic solvents presents difficulties for high speed industrial printing line development.^{3,4}

Water dispersed nanoparticles of conducting polymers, which can be readily synthesized using the miniemulsion technique, have been previously explored as materials for use in OPVs.⁵ More recently, roll-to-roll processing of water-dispersed nanoparticulate (NP) polymer solar cells has also been demonstrated for a range of low band gap materials.⁶ However, devices fabricated from aqueous nanoparticulate dispersions have traditionally exhibited lower efficiency than the corresponding bulk heterojunction (BHJ) devices, which has been ascribed to non-optimum film morphology.⁶

It is well established that the choice of cathode material plays a critical role in determining the efficiency of OPV devices.⁷ The work function of the cathode determines the internal electric field in the device and thus needs to be well matched to the LUMO of the electron accepting material to ensure facile electron transfer to the external circuit.⁸ Moreover, the effect of interfacial states, which can be created by chemical reactions (or other charge transfer processes) at the polymer/cathode interface, are complex and can be either detrimental or beneficial to device performance.⁸

In this Letter, we show that multilayered photovoltaic devices can be fabricated from aqueous nanoparticle dispersions (solar paint) that are more efficient than the corresponding bulk heterojunction blend devices. Furthermore, we compare the effect of Ca and Al cathodes (two of the most common electrode materials) in OPV devices based on polyfluorene blend aqueous polymer NP dispersions. The use of Ca/Al cathodes instead of Al cathodes results in a doubling of the efficiency of NP devices, which arises from reduced recombination.

An aqueous dispersion of semi-conducting PFB:F8BT (American Dye Source Inc) nanoparticles (1:1 blend) was prepared using the miniemulsion technique as outlined previously.⁹ Dynamic light scattering (Zetasizer Nano-ZS, Malvern Instruments, UK) was used to measure the distribution of particle sizes in the aqueous dispersion and gave a mean particle size of 51.9 ± 1.3 nm. Poly(3,4-ethylenedioxythiophene) poly(styrenesulfonate) (PEDOT:PSS) (Baytron P) films were spin-coated (5000 rpm) on pre-cleaned patterned indium tin oxide (ITO) glass slides and annealed at 140 °C for 30 min to eliminate water in the films. PFB:F8BT nanoparticle layers were deposited by spin coating 35 μ l of the dispersion (2000 rpm for 1 min) in air. Following the deposition of each layer, the film was dried at 70 °C for 15 min. After depositing the final layer, the films were dried at 140 °C for 15 min and then transferred into a vacuum chamber for cathode evaporation. Bulk heterojunction layers were spin coated from PFB:F8BT blend solutions (1:1 PFB:F8BT, 10 mg/ml in CHCl₃) to give a total layer thickness of approximately 110–120 nm as measured using a KLA-Tencor Alpha-step 500 surface profilometer. In comparison with the smooth intermixed BHJ films, previous atomic force microscopy studies have shown that the NP films adopt a random close packed structure.¹⁰ The calcium/aluminium (Ca/Al) and aluminium (Al) electrodes were evaporated on the active layers in vacuum (2×10^{-6} Torr). The thickness of the Ca and Al layers were measured to be about 20 nm and 70 nm, respectively, using a quartz crystal monitor. After evaporation, fabricated devices were annealed at 140 °C on a hot plate for 4 min under a nitrogen atmosphere and then tested. The photocurrent density-voltage (J-V) measurements were conducted using a Newport Class A solar simulator with an AM1.5 spectrum filter. The light intensity was measured to be 100 mW cm⁻² by a silicon reference solar cell (FHG-ISE) and the J-V data were recorded with a Keithley 2400 source meter.

Figure 1 shows that NP devices with Al and Ca/Al cathodes exhibit qualitatively very similar behavior, with a peak power conversion efficiency (PCE) of ~0.4% for Al and ~0.8% for Ca/Al, and that there is a distinct optimized thickness for the NP devices. The optimal thickness is a consequence of the competing physical effects of the repair and filling of defects for thin films^{11,12} and the development of

^{a)}Email: Paul.Dastoor@newcastle.edu.au. Tel.: +61-2-4921 5426. Fax: +61-2-4921 6907.

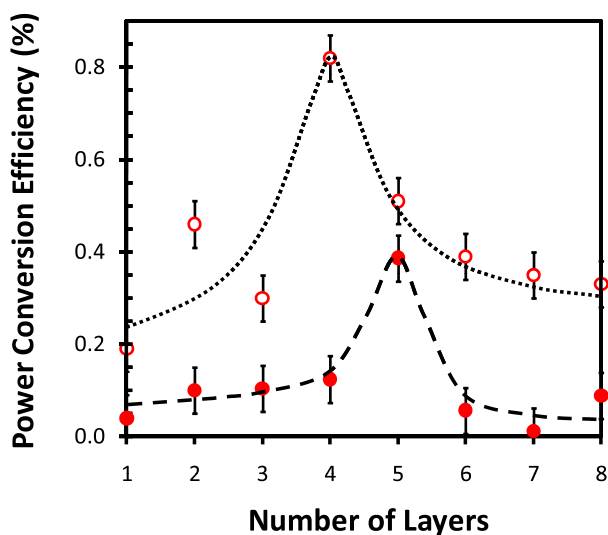


FIG. 1. Variation of PCE with number of deposited layers for PFB:F8BT nanoparticulate OPV devices fabricated with an Al cathode (filled circles) and a Ca/Al cathode (open circles). Dotted and dashed lines have been added to guide the eye. An average error has been determined based upon the variance for a minimum of ten devices for each number of layers.

stress cracking in thick films.¹³ Indeed, recent work by the authors has shown that the optimal layer thickness in these devices corresponds to the critical cracking thickness (CCT) above which stress cracking occurs resulting in low shunt resistance and a reduction in device performance.¹⁰

The J-V characteristics under illumination and the solar cell performance (for NP and BHJ devices for both cathodes) are summarized in Figure 2 and Table I, respectively. Despite being fabricated from a water-based system, the devices are stable and do not exhibit any rapid degradation of device characteristics in oxygen free conditions. The data show that: (a) changing from an Al to a Ca/Al electrode results in an approximate doubling of the measured PCE for both the NP and BHJ devices, and (b) the PCE of the NP devices is double that of the corresponding BHJ devices for both Al and Ca/Al cathodes.

The increased PCE of the NP devices relative to the BHJ devices is driven primarily by a significant increase in J_{sc} and demonstrates that this improvement is inherent to the NP structure and is not dependent upon the choice of cathode material. In addition, this PCE increase is not due to increased thickness of the NP devices, since the efficiency of F8BT:PFB BHJ devices is effectively constant for thicknesses between 50–500 nm (not shown). We have previously shown that the NPs have a phase-segregated core-shell domain structure with length scales close to the optimal size for exciton dissociation for the PFB-F8BT system.⁹ Thus, we

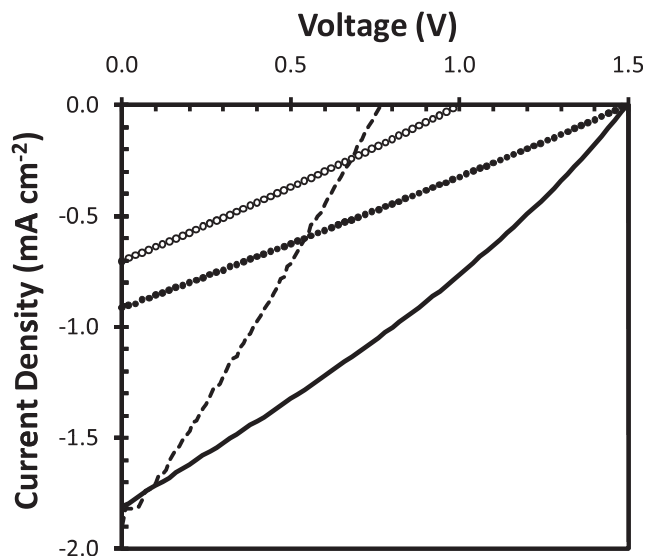


FIG. 2. Variation of current density as a function of applied voltage (J-V) for the most efficient PFB:F8BT 1:1 NP devices fabricated with Ca/Al (4 NP layers, solid line) and Al (5 NP layers, dashed line) cathodes. Also plotted are the J-V curves for PFB:F8BT 1:1 BHJ devices fabricated with Ca/Al (filled circles) and Al (open circles) cathodes.

hypothesise that the improved PCE of the NP devices arises from enhanced exciton dissociation resulting from an optimized domain structure in the NP active layer; a result not achievable by simple blending of bulk materials.¹⁴ Moreover, the low R_s values for the NP structures indicates that the charge transport pathways are not detrimentally affected by the nanoparticulate structure and interparticle connectivity must be high.

The NP devices with an Al cathode exhibit a significantly lower V_{oc} than the corresponding BHJ devices, which can be attributed to increased recombination.¹⁵ By contrast, the use of a Ca/Al cathode restores V_{oc} to the value observed for an optimized BHJ device whilst retaining the high J_{sc} values expected from the NP structure suggesting that the addition of calcium reduces recombination without detrimentally affecting charge generation and transport in the device. This result is consistent with previous observations that have shown that electron transfer occurs at the Ca/polymer interface resulting in a decrease in the HOMO of the polymer and an increase in V_{oc} .^{16,17}

The external quantum efficiency (EQE) spectra (Fig. 3) for the BHJ and NP devices are consistent with the device characteristics and, moreover, the J_{sc} values obtained under AM1.5 illumination agree with those obtained by combining the measured EQE spectra with the AM1.5 spectrum (J_{sc}^{EQE})

TABLE I. Comparison of device characteristics for the most efficient PFB:F8BT 1:1 NP devices fabricated with Ca/Al (4 NP layers) and Al (5 NP layers) cathodes and the corresponding BHJ devices. The data presented are for the best device of a minimum of ten devices and the Δ PCE error is obtained from the standard deviation of the device efficiencies. The J_{sc}^{EQE} values are calculated from the calibrated short circuit currents obtained by combining the measured EQE spectra with the AM1.5 spectrum (J_{sc}^{EQE}) (see supplementary material).

Type	Electrode	V_{oc} (V)	J_{sc} (mA/cm ²)	J_{sc}^{EQE} (mA/cm ²)	FF	PCE (%)	Δ PCE (%)	R_s (k Ω)	R_{sh} (k Ω)
NP	Ca/Al	1.50	1.81	1.91	0.30	0.82	0.05	4.3	21.0
NP	Al	0.77	1.81	1.72	0.28	0.39	0.03	2.0	18.1
BHJ	Ca/Al	1.48	0.91	0.91	0.27	0.36	0.02	26.6	39.1
BHJ	Al	1.00	0.71	0.84	0.26	0.19	0.02	23.3	37.3

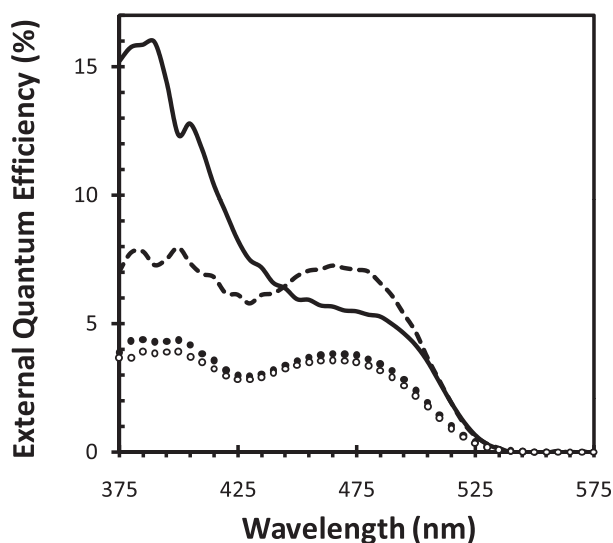


FIG. 3. EQE as a function of incident wavelength for PFB:F8BT 1:1 NP devices fabricated with Ca/Al (4 NP layers, solid line) and Al (5 NP layers, dashed line) cathodes. Also plotted are the EQE spectra for PFB:F8BT 1:1 BHJ devices fabricated with Ca/Al (filled circles) and Al (open circles) cathodes.

with an average deviation of less than $\pm 5\%$ (see supplementary material).²⁴ However, the different shapes of the NP EQE plots reveal that for the Ca/Al cathode NP device, there is a significantly increased contribution from charges generated by the PFB component (peak ~ 380 nm¹⁸). The active layer thicknesses of the np devices fabricated with either an Al or a Ca/Al cathode are the same and the thickness of the Ca layer is only 10 nm ($\sim 5\%$ of the wavelength of the peak absorption at 380 nm). As such, there is no mechanism whereby the observed EQE enhancement in the device with a Ca/Al could be due to either: (a) an antibatic response arising from a difference in device thickness or (b) a difference in the optical field distribution in the device due to

interference effects.¹⁹ We have previously established that PFB:F8BT NPs adopt a core shell morphology with a majority PFB component located in the shell.⁹ Westenhoff *et al.* has shown that immobile, metastable interfacial states are the bottleneck of device efficiency in blends of F8BT and PFB, with 75% of charge pairs rapidly recombining where they are formed resulting in a typically modest quantum efficiency (QE) of $\sim 3.4\%$.²⁰ As such, the increased PFB contribution to the EQE spectrum (maximum QE $\sim 16\%$) indicates that Ca must decrease the recombination of charges generated by the PFB component.

While there is likely to exist a rich complexity of interfacial structure and interactions in these devices, our results are consistent with a model (Figure 4) whereby Ca penetrates into the multilayered structure creating interfacial states at the surface of the NP. Ca readily penetrates polyfluorene films and significantly decreases the luminescence efficiency by rapidly quenching excitons that arrive at the calcium-polymer interface.²¹ Moreover, Ca doping of polyfluorene is known to create interband-gap states by lowering the energy of the frontier orbitals by up to 1.6 eV.¹⁶ Here, we propose that these states are created primarily in the PFB component, since this polymer preferentially segregates to the surface of the nanoparticle.⁹ Subsequently, electron transfer from Ca (Figure 4(b)) to the doped polymer (PFB*) results in a filled interband-gap state at the Ca-NP interface;²² excitons approaching these interband-gap states are likely to dissociate and contribute their holes to the polaron.²¹ For an exciton generated on PFB (Figure 4(c)), holes moving into the filled interband state create excess energy, which is transferred to the electron to conserve pair energy,²³ resulting in enhanced charge separation, and the observed increase in EQE contribution from PFB. Furthermore, the observed increase in V_{oc} for the calcium doped devices is explained by the reduction in PFB HOMO energy level.¹⁷ By contrast, for an exciton generated on F8BT, electron transfer to either the higher energy PFB LUMO or the filled lower energy PFB*

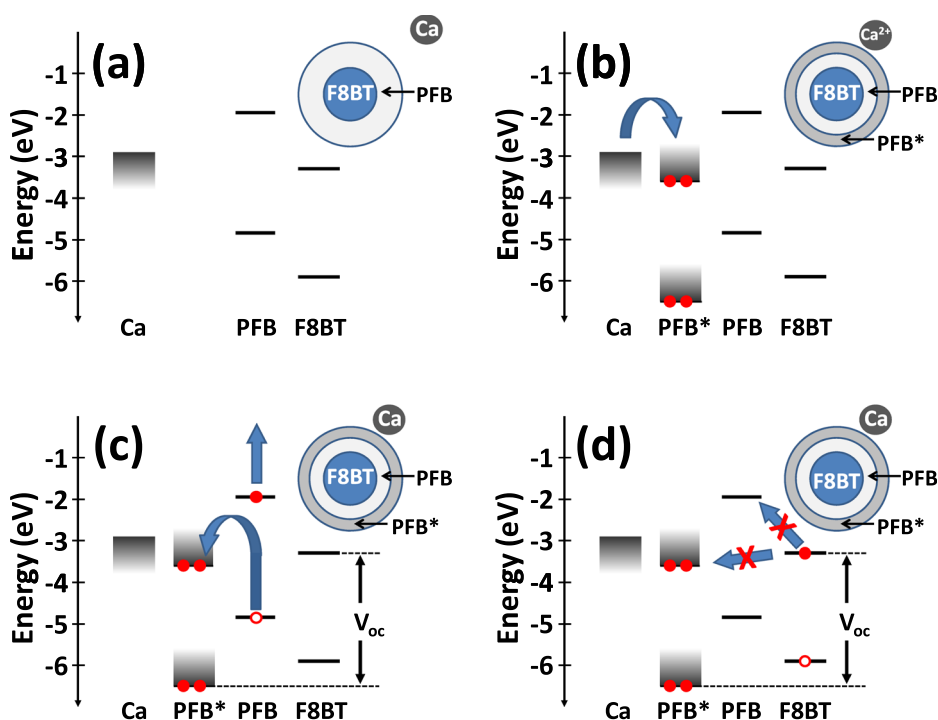


FIG. 4. Energy level diagrams for PFB:F8BT nanoparticles in the presence of calcium. (a) Calcium diffuses to nanoparticle surface. (b) Calcium dopes PFB-rich shell producing gap states. Electron transfer occurs from calcium producing filled gap states. (c) An exciton generated on PFB approaches the doped PFB material (PFB*) and a hole transfers to the filled gap state producing a more energetic electron. (d) Electron transfer from an exciton generated on F8BT to either the higher energy PFB LUMO or the filled lower energy PFB* LUMO is hindered.

LUMO or the filled lower energy PFB* LUMO is unfavourable (Figure 4(d)). Thus, regions of the PFB-rich shell that are Ca-doped act as a partial blocking layer for charges generated on the F8BT explaining the reduced EQE contribution from this component. Furthermore, any Ca-doping of the minority F8BT in the outer shell of the NP results in additional electron trap states at the interface.

In summary, we have shown that the intrinsic morphology of NP PFB:F8BT OPV devices enhances exciton dissociation relative to the corresponding BHJ structure. Moreover, the use of a Ca/Al cathode results in the creation of interfacial gap states, which reduce recombination of charges generated by the PFB in these devices and restores V_{oc} to the level obtained for an optimized BHJ device, resulting in a PCE approaching 1%.

The University of Newcastle is gratefully acknowledged for Ph.D. scholarships (B.V. and A.S.).

- ¹B. Azzopardi, C. J. M. Emmott, A. Urbina, F. C. Krebs, J. Mutale, and J. Nelson, *Energy Environ. Sci.* **4**, 3741 (2011).
²K. C. Krebs, *Sol. Energy Mater. Sol. Cells* **93**, 394 (2009).
³A. M. Ruder, *Ann. N.Y. Acad. Sci.* **1076**, 207 (2006).
⁴E. M. Ward, P. A. Schulte, K. Straif, N. B. Hopf, J. C. Caldwell, T. Carreón, D. M. DeMarini, B. A. Fowler, B. D. Goldstein, K. Hemminki, C. J. Hines, K. H. Pursiainen, E. Kuempel, J. Lewtas, R. M. Lunn, E. Lyng, D. M. McElvenny, H. Muhle, T. Nakajima, L. W. Robertson, N. Rothman, A. M. Ruder, M. K. Schubauer-Berigan, J. Siemiatycki, D. Silverman, M. T. Smith, T. Sorahan, K. Steenland, R. G. Stevens, P. Vineis, S. H. Zahm, L. Zeise, and V. J. Cogliano, *Environ. Health Perspect.* **118**, 1355 (2010).
⁵K. Landfester, R. Montenegro, U. Scherf, R. Güntner, U. Asawapirom, S. Patil, D. Neher, and T. Kietzke, *Adv. Mater.* **14**, 651–655 (2002).
⁶T. R. Andersen, T. T. Larsen-Olsen, B. Andreasen, A. P. L. Böttiger, J. E. Carlé, M. Helgesen, E. Bundgaard, K. Norrman, J. W. Andreasen, M. Jørgensen, and F. C. Krebs, *ACS Nano* **5**, 4188–4196 (2011).

- ⁷C. J. Brabec, A. Cravino, D. Meissner, N. S. Sariciftci, T. Fromherz, M. T. Rispens, L. Sanchez, and J. C. Hummelen, *Adv. Funct. Mater.* **11**, 374 (2001).
⁸M. O. Reese, M. S. White, G. Rumbles, D. S. Ginley, and S. E. Shaheen, *Appl. Phys. Lett.* **92**, 053307 (2008).
⁹K. B. Burke, A. J. Stapleton, B. Vaughan, X. Zhou, A. L. D. Kilcoyne, W. J. Belcher, and P. C. Dastoor, *Nanotechnology* **22**, 265710 (2011).
¹⁰A. Stapleton, B. Vaughan, B. Xue, E. Sesa, K. Burke, X. Zhou, G. Bryant, O. Werzer, A. Nelson, A. L. D. Kilcoyne, L. Thomsen, E. Wanless, W. Belcher, and P. Dastoor, *Sol. Energy Mater. Sol. Cells* **102**, 114 (2012).
¹¹P. A. Steward, J. Hearn, and M. C. Wilkinson, *Adv. Colloid Interface Sci.* **86**, 195 (2000).
¹²S. V. Karpov, I. L. Isaev, A. P. Gavriluk, V. S. Gerasimov, and A. S. Grachev, *Colloid* **71**, 329 (2009).
¹³K. Singh and M. Tirumkudulu, *Phys. Rev. Lett.* **98**, 218302 (2007).
¹⁴C. R. McNeill, S. Westenhoff, C. Groves, R. H. Friend, and N. C. Greenham, *J. Phys. Chem. C* **111**, 19153 (2007).
¹⁵L. J. A. Koster, V. D. Mihailetschi, R. Ramaker, and P. W. M. Blom, *Appl. Phys. Lett.* **86**, 123509 (2005).
¹⁶L. S. Liao, L. F. Cheng, M. K. Fung, C. S. Lee, S. T. Lee, M. Inbasekaran, E. P. Woo, and W. W. Wu, *Phys. Rev. B* **62**, 10004 (2000).
¹⁷W.-H. Tseng, M.-H. Chen, J.-Y. Wang, C.-T. Tseng, H. Lo, P.-S. Wang, and C.-I. Wu, *Sol. Energy Mater. Sol. Cells* **95**, 3424 (2011).
¹⁸C. R. McNeill, H. Frohne, J. L. Holdsworth, and P. C. Dastoor, *Nano Lett.* **4**, 2503 (2004).
¹⁹N. Nicolaidis, B. Routley, J. Holdsworth, W. Belcher, X. Zhou, and P. Dastoor, *J. Phys Chem C* **115**, 7801 (2011).
²⁰S. Westenhoff, I. A. Howard, J. M. Hodgkiss, K. R. Kirov, H. A. Bronstein, C. K. Williams, N. C. Greenham, and R. H. Friend, *J. Am. Chem. Soc.* **130**, 13653 (2008).
²¹M. Stoessel, G. Wittmann, J. Staudigel, F. Steuber, J. Blässing, W. Roth, H. Klausmann, W. Rogler, J. Simmerer, A. Winnacker, M. Inbasekaran, and E. P. Woo, *J. Appl. Phys.* **87**, 4467 (2000).
²²Y. Park, V.-E. Choong, B. R. Hsieh, C.W. Tang, and Y. Gao, *Phys. Rev. Lett.* **78**, 3955 (1997).
²³M. J. Rice and Y. N. Garstein, *Phys. Rev. B* **53**, 10764 (1996).
²⁴See supplementary material at <http://dx.doi.org/10.1063/1.4737640> for a comparison of the integrated J_{sc} obtained from the EQE spectra with the J_{sc} obtained under AM1.5 conditions for PFB:F8BT blend devices.